

Showcasing research from the group of Dr Kwang-Ryeol Lee and Dr Xiaowei Li, Computational Science Center, Korea Institute of Science and Technology, South Korea

Transformation of amorphous carbon to graphene on low-index Ni surfaces during rapid thermal processing: a reactive molecular dynamics study

This computational work explored the transformation of amorphous carbon to graphene on different Ni surfaces during rapid thermal processing using reactive molecular dynamics simulation. Our simulation results showed that due to the difference in activation energy, Ni surfaces affected the diffusion behavior of C into Ni and thus modulated the remnant number of C atoms, dominating the formation and quality of graphene, which accorded with the developed empirical equation.

### As featured in:



See Xiaowei Li, Kwang-Ryeol Lee *et al.*, *Phys. Chem. Chem. Phys.*, 2019, 21, 2271.



ROYAL SOCIETY  
OF CHEMISTRY

Celebrating  
IYPT 2019

[rsc.li/pccp](http://rsc.li/pccp)

Registered charity number: 207890

Cite this: *Phys. Chem. Chem. Phys.*, 2019, 21, 2271Received 8th October 2018,  
Accepted 6th November 2018

DOI: 10.1039/c8cp06218h

rsc.li/pccp

# Transformation of amorphous carbon to graphene on low-index Ni surfaces during rapid thermal processing: a reactive molecular dynamics study

Xiaowei Li,<sup>ib</sup>\*<sup>ab</sup> Aiyang Wang<sup>b</sup> and Kwang-Ryeol Lee\*<sup>a</sup>

**The transformation of amorphous carbon to graphene on different Ni surfaces during rapid thermal processing was explored using reactive molecular dynamics simulation. Due to the difference in activation energy, Ni surfaces affected the diffusion behavior of C into Ni and thus modulated the remnant number of C atoms, dominating the formation and quality of graphene, which accorded with the developed empirical equation.**

A fast transfer-free synthesis of graphene on a dielectric substrate can be achieved *via* the metal-catalyzed solid-state transformation of amorphous carbon (a-C) using rapid thermal processing (RTP).<sup>1–4</sup> This provides a clean and crackless route to synthesize high-quality graphene on any possible dielectric substrate directly. In particular, the presence of catalytically active transition metals, such as Ni,<sup>1,3–5</sup> Cu,<sup>2</sup> Fe,<sup>4</sup> *etc.*, plays a key role in the graphene growth, among which Ni is commonly considered as a strong candidate owing to its catalytic capability and the dissolution of C into Ni.<sup>1,3–5</sup>

Nickel's role as the catalyst of choice, which was widely employed in the graphene fabrication through the chemical vapor deposition (CVD) method,<sup>6–8</sup> has been extensively studied *via* experimental<sup>6–8</sup> and theoretical techniques,<sup>9–11</sup> providing in-depth information on the adsorption, decomposition, reformation, and desorption of various hydrocarbon species on the Ni surface. Especially, previous efforts<sup>12–14</sup> reported that the different low-index Ni surfaces, such as (100), (110), and (111), were of different reactive activities, which affected not only the chemisorption barrier for hydrocarbon onto Ni but also the cleavage of C–H bonds and the formation of C–C bonds for graphene growth. However, for the a-C-to-graphene transformation during the RTP process, the diffusion barrier of C into Ni is also closely related with Ni surfaces, while the fundamental

understanding of the diffusion behavior of C and Ni atoms and graphene formation on these low-index Ni surfaces is still not clarified yet, which is essential to the high-quality synthesis of graphene on a large scale.

In the present work, we carried out reactive molecular dynamics (RMD) calculations to simulate the Ni-catalyzed transformation of a-C to graphene *via* the RTP approach, and comparatively explored the effect of different Ni surfaces ((100), (110), and (111)) on the diffusion behavior of C into Ni and the graphene quality. All calculations were implemented using the LAMMPS code.<sup>15</sup> Fig. 1 shows the two-layer model, composed of a-C and crystalline Ni (Ni@a-C). The a-C with a density of 3.22 g cm<sup>−3</sup> and a size of 30.672 × 26.06 × 8.4 Å<sup>3</sup> was fabricated using a liquid-quenching method by *ab initio* MD simulation,<sup>16,17</sup> which contained 872 C atoms, an sp<sup>3</sup> fraction of 63.3 at%, and an sp<sup>2</sup> fraction of 25.7 at%. For the Ni layer, the Ni(111) (144 Ni atoms per atom layer), Ni(110) (90 Ni atoms per atom layer), and Ni(100) (120 Ni atoms per atom layer) were adopted separately, and the number of Ni atoms was fixed at 2880 for each case. The mismatches between the a-C and Ni(111), Ni(110), or Ni(100) layers in *x* and *y* directions were less than 4.6%, and the initial distance between the Ni and a-C layers was 2 Å. In order to study the diffusion behavior of Ni and C atoms in the system, there was no layer fixed during the RTP process.<sup>18</sup> A vacuum with a thickness of about 35 Å above the Ni top surface was used for each case,

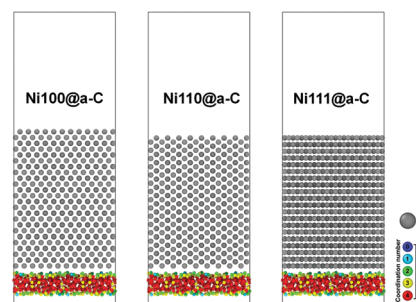


Fig. 1 Simulation models of Ni100@a-C, Ni110@a-C, and Ni111@a-C.

<sup>a</sup> Computational Science Center, Korea Institute of Science and Technology, Seoul 136-791, Republic of Korea. E-mail: lixw0826@gmail.com, krlee@kist.re.kr

<sup>b</sup> Key Laboratory of Marine Materials and Related Technologies, Zhejiang Key Laboratory of Marine Materials and Protective Technologies, Ningbo Institute of Materials Technology and Engineering, Chinese Academy of Sciences, Ningbo 315201, P. R. China

the time step was 0.25 fs, and the periodic boundary conditions were employed along the  $x$  and  $y$  directions.

ReaxFF potential developed by Mueller *et al.*<sup>12</sup> was adopted to describe the C–Ni interaction, and its reliability for our simulated system has been further validated by the additional ReaxFF MD and *ab initio* calculations. During the RTP process, the temperature of the system increased from 300 to 1800 K first by a stepwise heating method<sup>17,18</sup> using the *NVT* ensemble with a Nosé–Hoover thermostat,<sup>19</sup> and 100 ps was given for each temperature to relax the system; after that, the diffusion at 1800 K for 1350 ps was undertaken to explore the diffusion behavior of C into the Ni layer and the a-C structural transformation during the short MD simulation time. 1800 K was appropriate to observe the obvious diffusion behavior of C and Ni atoms without significant graphitic dissolution, although it was much higher than the experimental values<sup>1–5,20</sup> because of the inevitable existence of Ni defects and the surface/interface contamination.

Fig. 2 shows the change of morphologies with diffusion time at 1800 K. For each system, when the temperature increases from 300 to 1800 K (0 ps), only a few C and Ni atoms interact with each other to form a fuzzy interface, while most of the Ni atoms only slightly deviate from their equilibrium positions due to the high temperature rather than the significant melting.<sup>18</sup> As the diffusion time elapses from 0 to 1350 ps at 1800 K, more C atoms diffuse into the Ni layer to form the C–Ni intermixing region, while the remnant a-C evolves into a graphene structure. However, different diffusion behaviors are observed under different Ni surface conditions. For the Ni100@a-C system, after diffusion at 1800 K for 1350 ps, all Ni atoms participate in the diffusion process, and the crystal character of the Ni layer disappears instead of the viscous liquid-like state due to the C dissolution reducing the melting point of the Ni layer.<sup>1,18</sup> When Ni(100) is replaced with Ni(110) and Ni(111), respectively, besides the formed graphene and C–Ni intermixing region, Ni atoms still partially remain, which still maintain a crystal-like structure, indicating the high diffusion barrier and structural stability.<sup>12,21</sup> This suggests the different diffusion rates when the Ni surface ranges from (100) to (110) and (111), which will be discussed later.

In order to evaluate the diffusion behavior of C and Ni atoms during the RTP process, the mean square displacement (MSD) with time is calculated for each case (Fig. 3a) using the following equation:<sup>22</sup>

$$\text{MSD} = r^2(t) = \frac{1}{N} \left\langle \sum_{i=1}^N |r_i(t) - r_i(0)|^2 \right\rangle \quad (1)$$

where  $N$  is the number of  $i$  atoms in the system;  $r_i(0)$  and  $r_i(t)$  are the positions of the  $i$  atom at times of 0 and  $t$ , respectively. When the temperature is smaller than 1800 K, the MSD changes slightly for each case, while it increases drastically at the temperature higher than 1800 K, agreeing well with the change of morphologies (Fig. 2). In particular, different diffusion rates are observed for each case. First, the diffusion rate of C is higher than that of Ni for each case. However, when the Ni surface varies from (100) to (110) and (111), the diffusion rates of both C and Ni decrease, leading to fewer C atoms diffused into Ni layers, which is confirmed by the narrow intermixing region (Fig. 2). This indicates that for the a-C-to-graphene transformation during the RTP process, the remnant number of C atoms after diffusion at 1800 K is affected by the selected Ni surface, dominating the formation time of the graphene structure by tailoring the diffusion rates of C.

Previous study<sup>12</sup> reported that the Ni(111) surface was the least reactive of the low index surfaces and had high stability, while Ni(100) had the fastest reaction rate with other species. In order to further evaluate the energy barrier for C diffusion from the a-C layer into different Ni layers and quantify the effect of different Ni surfaces on diffusion behavior, we further calculate the activation energy for C diffusion according to the following equations:

$$\text{MSD} = 6Dt \quad (2)$$

$$D = D_0 \exp\left(-\frac{Q}{RT}\right) \quad (3)$$

$$\ln D = \ln D_0 - \frac{Q}{RT} \quad (4)$$

where  $D$  is the diffusion coefficient ( $\text{m}^2 \text{s}^{-1}$ ),  $D_0$  is diffusion constant,  $R$  is a constant value ( $8.314 \text{ J} (\text{mol K})^{-1}$ ),  $T$  is the

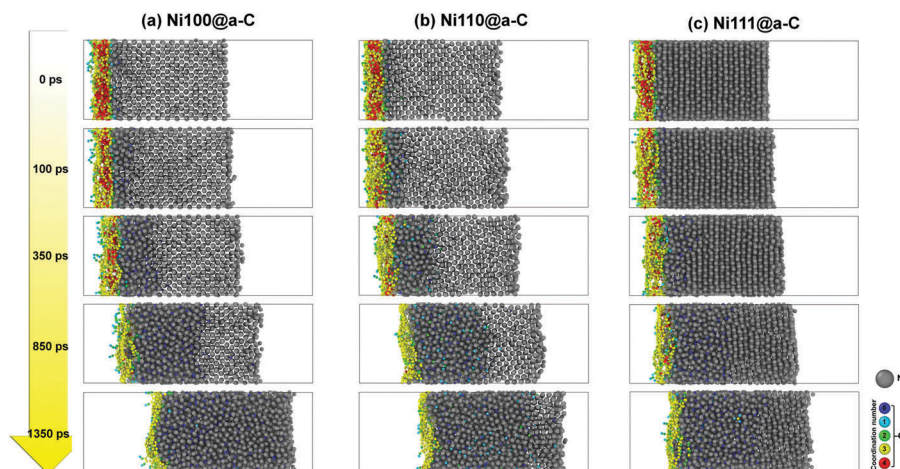


Fig. 2 Morphologies during the diffusion time of 1350 ps at 1800 K for (a) Ni100@a-C, (b) Ni110@a-C, and (c) Ni111@a-C systems, respectively.

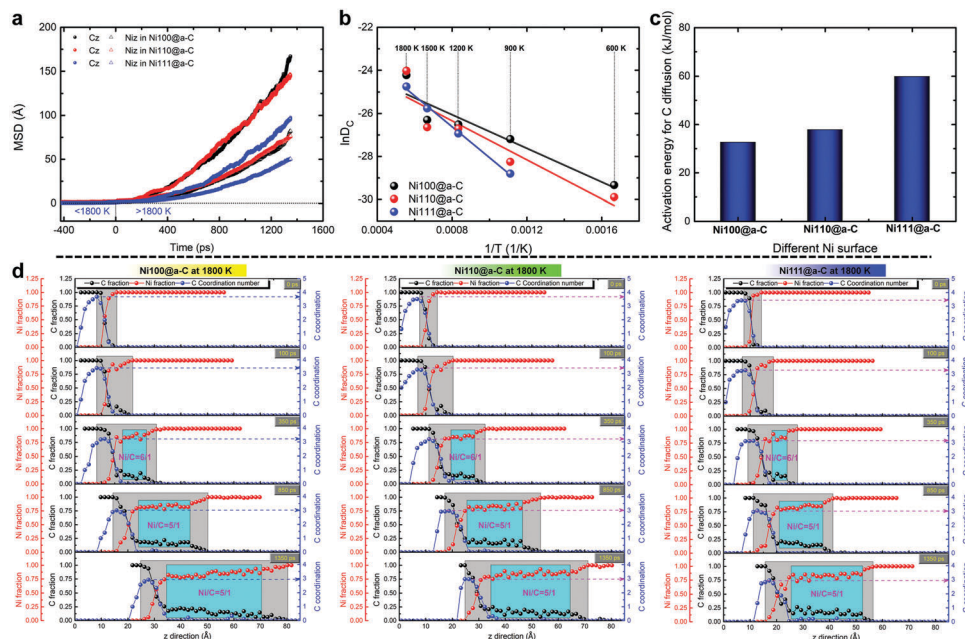


Fig. 3 (a) MSD of C and Ni atoms with diffusion time, (b) relationship between the diffusion coefficient of C and  $1/T$ , (c) calculated activation energy for C diffusion, and (d) profiles of C and Ni atomic fractions with diffusion time at 1800 K along the diffusion couple direction when the Ni surface changes from (100) to (110) and (111), respectively.

absolute temperature (K), and  $Q$  is the activation energy for diffusion ( $\text{J mol}^{-1}$ ). First, the diffusion coefficient of C atoms is obtained by fitting the MSD for each temperature according to eqn (2),<sup>18</sup> and then the relationship between the  $\ln D$  and  $1/T$  is plotted, as shown in Fig. 3b. By further linear fitting according to eqn (4), the activation energies for C diffusion in Ni100@a-C, Ni110@a-C, and Ni111@a-C systems are estimated (Fig. 3c), which are 32.6, 37.8, and 59.8  $\text{kJ mol}^{-1}$ , respectively. The difference in activation energies could account for the distinct diffusion rates of C into Ni layers and the width of the C–Ni intermixing region, which is consistent with the previous report.<sup>12</sup> However, it should be mentioned that the values in Fig. 3c can be changed in experiments and calculations due to the existence of grain boundaries and defects in the Ni layer and the variation of the a-C structure.<sup>14</sup>

Moreover, Fig. 3d gives the profiles of C and Ni atomic fractions with diffusion time at 1800 K along the diffusion couple direction, when the Ni surface is (100), (110), or (111), respectively. It reveals that due to the different diffusion rates of C and Ni atoms, the difference in the C–Ni intermixing width is further confirmed. A plateau region with the Ni/C atomic ratio of 5/1 is produced for each case after 1350 ps at 1800 K, displaying the viscous liquid-like character,<sup>18</sup> and the width of the plateau region becomes broader as the Ni surface goes from (111) to (100). In particular, note that once the Ni/C atomic ratio of 5/1 in the plateau region is formed, further extending the diffusion time has no effect on the Ni/C atomic ratio but only increases the width of the plateau region.

The graphene structure obtained for each case is analyzed systematically to evaluate the difference in quality caused by Ni surfaces. Fig. 4a illustrates the graphene images obtained for

each case after the diffusion time of 1350 ps. When the Ni surface varies from (100) to (110) and (111), the remnant C atoms near the a-C side are catalyzed by Ni to form the graphene structure, rather than undergoing the dissolution/precipitation mechanism typically involved in Ni-catalyzed CVD growth of graphene,<sup>6–8,14</sup> the difference in the number of C atoms, induced by different Ni surfaces, results in the graphene layers being changed from a single-layer to multilayers. In addition, there are many defects observed due to the limited MD simulation time, which can be reduced drastically by extending the diffusion time or increasing the heating temperature.<sup>20</sup>

For each system, the number of C and Ni atoms in the red square regions in the inset images of Fig. 4b, including graphene, transition, and C–Ni intermixing regions, are summed separately, and then the relationship between them is plotted, as shown in Fig. 4b. Note that the transformation of a-C to the graphene structure, obtained from the Ni@a-C systems with different Ni surfaces, can also be described accurately by the following empirical equation developed in our previous study (manuscript under preparation).

$$N_C = \frac{1}{5}N_{\text{Ni}} + 305 \quad \text{For intact monolayer graphene} \quad (5)$$

$$N_C = \frac{1}{5}N_{\text{Ni}} + 610 \quad \text{For intact bilayer graphene} \quad (6)$$

where  $N_{\text{Ni}}$  is the number of Ni atoms in the system;  $N_C$  is the number of C atoms in the system; the constant values, 305 and 610, are the required number of C atoms to form the perfect monolayer and bilayer graphenes, respectively, according to the present system size. After the same diffusion time (1350 ps), the position for the Ni100@a-C system is more close to the line for

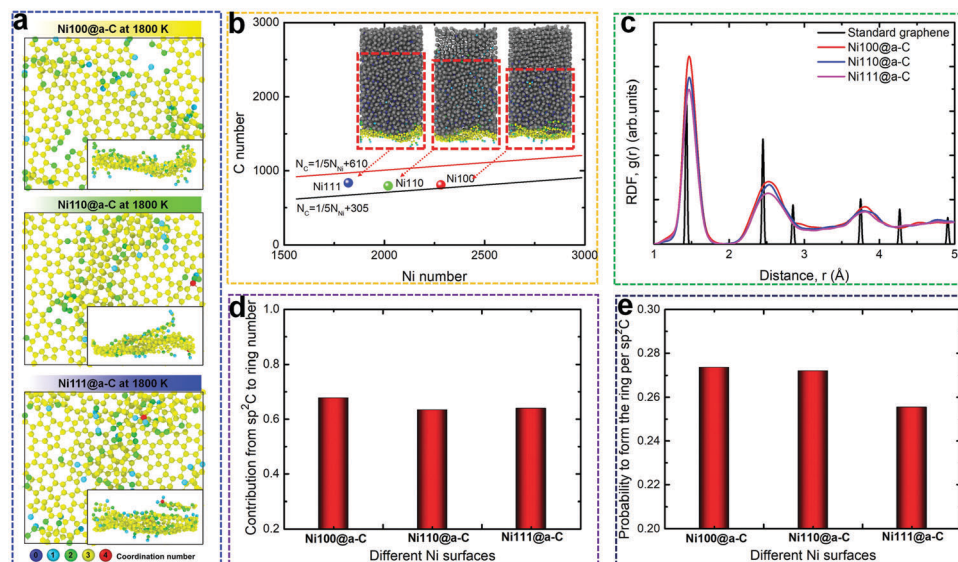


Fig. 4 Structural analysis of graphene obtained for each case, including (a) images of the graphene structure after diffusion time of 1350 ps at 1800 K, (b) relationship between the number of C and Ni atoms in the red square regions in the inset images, (c) RDF spectra, (d) proportion of  $sp^2C$  contribution to the number of rings including 5, 6, and 7-membered cases, and (e) probability to form the ring structure per  $sp^2C$  atom.

the monolayer graphene; however, for Ni110@a-C and Ni111@a-C, they deviate to the line for bilayer graphene due to the large number of C atoms, which is in accordance with the result in Fig. 4a.

In order to evaluate the quality of the graphene structure, the radial distribution function (RDF) in Fig. 4c reveals that the regular arrangement is enhanced gradually with the Ni surface changing from (111) to (110) and (100). Furthermore, the numbers of 5, 6, and 7-membered rings are calculated, and the  $sp^2C$  contribution to the number of rings and the probability to form the ring per  $sp^2C$  atom are evaluated, as shown in Fig. 4d and e, which decrease clearly as the Ni surface changes from (100) to (110) and (111). These confirm the higher quality of the graphene structure obtained in the Ni100@a-C system than those obtained in Ni110@a-C and Ni111@a-C cases. However, it should be mentioned that if the diffusion time at 1800 K is further extended for Ni110@a-C and Ni111@a-C systems, the graphene with similar quality to that of Ni100@a-C should be obtained due to the further diffusion of C into the Ni layer.

In conclusion, we performed RMD simulations to study the dependence of a-C-to-graphene transformation on different low-index Ni surfaces during the RTP process. Our simulation suggested that Ni surfaces affected the diffusion behavior of C into Ni layers, and the Ni100@a-C system had the highest diffusion rates of C atoms than other cases due to the low activation energy for C diffusion. Diffusion rates resulted in the change of the remnant number of C atoms for the graphene formation, which decreased gradually as the Ni surface changed from (100) to (110) and (111), but the plateau region with the Ni/C atomic ratio of 5/1 was still observed for each case. In particular, the dependence of a-C-to-graphene transformation on Ni surfaces could also be explained by our developed empirical equation, indicating that the Ni100@a-C system exhibited the highest graphene quality compared to Ni111@a-C and Ni100@a-C

systems after the same diffusion time. This result discloses the fundamental understanding for the effect of Ni surfaces on the a-C-to-graphene transformation, and provides guidance to tailor the number of graphene layers formed on different Ni surfaces for various technological applications.

## Conflicts of interest

There are no conflicts to declare.

## Acknowledgements

This research was supported by the Korea Research Fellowship Program funded by the Ministry of Science and ICT through the National Research Foundation of Korea (2017H1D3A1A01055070), the Nano Materials Research Program through the Ministry of Science and IT Technology (NRF-2016M3A7B4025402), and the National Natural Science Foundation of China (51772307 and 51522106).

## Notes and references

- W. Xiong, Y. S. Zhou, L. J. Jiang, A. Sarkar, M. Mahjouri-Samani, Z. Q. Xie, Y. Gao, N. J. Ianno, L. Jiang and Y. F. Lu, *Adv. Mater.*, 2013, **25**, 630–634.
- Z. Wu, Y. Guo, Y. Guo, R. Huang, S. Xu, J. Song, H. Lu, Z. Lin, Y. Han, H. Li, T. Han, J. Lin, Y. Wu, G. Long, Y. Cai, C. Cheng, D. Su, J. Robertson and N. Wang, *Nanoscale*, 2016, **8**, 2594–2600.
- M. Zheng, K. Takei, B. Hsia, H. Fang, X. Zhang, N. Ferralis, H. Ko, Y. L. Chueh, Y. Zhang, R. Maboudian and A. Javey, *Appl. Phys. Lett.*, 2010, **96**, 063110.
- J. A. Rodríguez-Manzo, C. Pham-Huu and F. Banhart, *ACS Nano*, 2011, **5**, 1529–1534.

- 5 H. Sun, X. Li, Y. Li, G. Chen, Z. Liu, F. E. Alam, D. Dai, L. Li, L. Tao, J. B. Xu, Y. Fang, X. Li, P. Zhao, N. Jiang, D. Chen and C. T. Lin, *Chem. Mater.*, 2017, **29**, 7808–7815.
- 6 J. Gong, Z. Liu, J. Yu, D. Dai, W. Dai, S. Du, C. Li, N. Jiang, Z. Zhan and C. T. Lin, *Composites, Part A*, 2016, **87**, 290–296.
- 7 T. Wu, Z. Liu, G. Chen, D. Dai, H. Sun, W. Dai, N. Jiang, Y. H. Jiang and C. T. Lin, *RSC Adv.*, 2016, **6**, 23956–23960.
- 8 A. Reina, X. Jia, J. Ho, D. Nezich, H. Son, V. Bulovic, M. S. Dresselhaus and J. Kong, *Nano Lett.*, 2009, **9**, 30–35.
- 9 L. Meng, Q. Sun, J. Wang and F. Ding, *J. Phys. Chem. C*, 2012, **116**, 6097–6102.
- 10 Z. Xu, T. Yan, G. Liu, G. Qiao and F. Ding, *Nanoscale*, 2016, **8**, 921–929.
- 11 Y. Wang, A. J. Page, Y. Nishimoto, H. J. Qian, K. Morokuma and S. Irle, *J. Am. Chem. Soc.*, 2011, **133**, 18837–18842.
- 12 J. E. Mueller, A. C. T. van Duin and W. A. Goddard III, *J. Phys. Chem. C*, 2010, **114**, 4939–4949.
- 13 H. L. Abbott, A. Burkoski, D. F. Kavulak and I. Harrison, *J. Chem. Phys.*, 2003, **119**, 6407–6410.
- 14 D. L. Mafra, J. A. Olmos-Asar, F. R. Negreiros, A. Reina, K. K. Kim, M. S. Dresselhaus, J. Kong, G. J. Mankey and P. T. Araujo, *Phys. Rev. Mater.*, 2018, **2**, 073404.
- 15 S. Plimpton, *J. Comput. Phys.*, 1995, **117**, 1–19.
- 16 X. Li, P. Guo, L. Sun, A. Wang and P. Ke, *ACS Appl. Mater. Interfaces*, 2015, **7**, 27878–27884.
- 17 X. Li, L. Li, D. Zhang and A. Wang, *ACS Appl. Mater. Interfaces*, 2017, **9**, 41116–41119.
- 18 S. Chen, W. Xiong, Y. S. Zhou, Y. F. Lu and X. C. Zeng, *Nanoscale*, 2016, **8**, 9746–9755.
- 19 D. J. Evans and B. L. Holian, *J. Chem. Phys.*, 1985, **83**, 4069–4074.
- 20 A. Barreiro, F. Börrnert, S. M. Avdoshenko, B. Rellinghaus, G. Cuniberti, M. H. Rummeli and L. M. K. Vandersypen, *Sci. Rep.*, 2013, **3**, 1115.
- 21 T. P. Beebe, D. W. Goodman, B. D. Kay and J. D. Yates, *J. Chem. Phys.*, 1987, **87**, 2305–2315.
- 22 D. Frenkel and B. Smit, *Understanding Molecular Simulation from Algorithms to Applications*, Academic Press, Orlando, USA, 1996.